Lithuanian Journal of Physics
Vol. **66**, No. 2, pp. 113–124 (2026)
ISSN 1648-8504 eISSN 2424-3647
DOI: https://doi.org/10.3952/physics.2026.66.2.6

A COMPUTATIONAL QM/MD ^{17}O NMR STUDY OF TAUTOMERIC EQUILIBRIUM OF MYCOTOXIN CITRININ IN DICHLOROMETHANE SOLUTION

Ž. Murnikova and K. Aidas

Institute of Chemical Physics, Faculty of Physics, Vilnius University, Saulėtekio 3, 10257 Vilnius, Lithuania
Email: kestutis.aidas@ff.vu.lt

Received 2 December 2025; accepted 21 January 2026

The tautomeric equilibrium of citrinin in dichloromethane was investigated using classical molecular dynamics and linear-response QM/MM calculations of ^{17}O NMR shielding constants. MD simulations showed that solvent distribution around the *para*- and *ortho*-quinone methide tautomers is essentially uniform, as expected for an isotropic non-hydrogen-bonding solvent of medium polarity. The tautomeric ratio between the *p*- and *o*-citrinin forms was optimized to best match experimental and computed relative ^{17}O NMR spectra. The resulting tautomeric ratio of *p*-to-*o*-citrinin of 7:4 closely reproduces the experimental value of 4:3, confirming the near-thermodynamic equivalence of the two tautomers, with a slight preference for the *para* form. A thermodynamic-cycle-based quantum-chemical estimate yielded virtually the same qualitative conclusion. Attempts to include the endiol tautomer of citrinin showed it to be unstable in a dielectric-continuum solvent model; thus, the endiol tautomer is not expected to form in dichloromethane and does not contribute to the observed NMR spectra.

Keywords: citrinin, tautomerism, nuclear magnetic resonance, molecular dynamics simulation, quantum mechanics/molecular mechanics

1. Introduction

Nuclear magnetic resonance (NMR) spectroscopy has long proven to be an invaluable and versatile tool in structural studies of a wide range of solid- and liquid-state materials [1–3] as well as of biological macromolecules [4, 5]. The shape of the high-resolution NMR spectra is, however, also dictated by the rate of the dynamical processes occurring in the sample on the molecular level. In the case of the so-called fast chemical exchange regime, the absorption peaks recorded in the NMR spectrum correspond to nuclear responses averaged over all states involved in the rapid interconversion, which is to be contrasted to the conditions of the slow exchange where a series of separate state-resolved signals from all magnetically inequivalent nuclei are normally recorded instead [6]. The fast exchange occurs when the rate of the interconversion between some states A and B, k, is much higher than the difference of the Larmor frequencies, ν_0, of the nucleus in these two states with the associated chemical shifts δ_A and δ_B – that is, $k \gg 2\pi\nu_0 |\delta_A - \delta_B|$. Typical examples of the fast chemical exchange include various conformational transitions, e.g. methyl group rotation, proton transfer reactions or ion pairing phenomena. Tautomerization reactions have been widely studied using NMR [7], and they usually also occur under conditions of the fast chemical exchange. In the case of the fast interconversion between tautomeric forms A and B, a single tautomer-averaged NMR spectrum is recorded where the observed chemical shifts δ^{obs} are given according to

$$\delta^{obs} = \chi_A \cdot \delta_A + \chi_B \cdot \delta_B. \quad (1)$$

In Eq. (1), quantities χ_A and χ_B are the relative equilibrium populations of tautomers A and B with $\chi_A + \chi_B = 1$. Thus, tautomeric equilibrium constants could be deduced from Eq. (1) provided that the NMR spectrum of every individual tautomer is known. However, these are seldom available

with the required precision. They could be measured by suppressing the tautomeric interconversion using appropriate chemical substitutions or shifting to some model systems or solid-phases where a single tautomer is predominant [7], yet the effects of these alterations on the NMR chemical shifts of the tautomers are non-negligible and can be hard to estimate or control.

An alternative route to achieve the NMR spectra of individual tautomeric forms is by using modern molecular modelling techniques based on quantum mechanics, see, for example, Refs. [8–11]. Because tautomeric interconversion is usually mediated by the environment, a reliable description of solute–solvent interactions ought to be incorporated into the electronic structure approach. Solvation models used in connection with the electronic structure methods can be generally categorized into implicit and explicit solvent models. The implicit solvent model such as, for example, the polarizable continuum model [12, 13] or the conductor-like screening model [14] considers the environment as a homogeneous medium that surrounds the solute within a molecule-shaped cavity. The explicit solvent model preserves the discrete nature of solvent molecules that can be treated at different levels of sophistication. Ideally, solvent molecules should be described using the same electronic structure method as that applied for the solute, a modelling scheme that has historically been termed as a supermolecular approach [15]. However, the severe scaling of the electronic structure methods does not allow including a sufficient number of solvent molecules around the solute to achieve the converged effect of electrostatic interactions, and therefore this model is only feasible by considering a small number of solvent molecules in the vicinity of the solute. Alternatively, the so-called combined quantum mechanics/molecular mechanics (QM/MM) models [16] could be utilized where the multipole expansion of the electronic density of the solvent molecules is considered instead. Polarizable QM/MM models have been developed as well where, in addition to the static multipole expansion, dipole–dipole polarizabilities are assigned to the molecules, leading to the explicit account of solute–solvent polarization interactions [17, 18]. Furthermore, solvent molecules in the vicinity of the solute can be described quantum mechanically, thus accounting for short-range intermolecular interactions of non-classical origin.

The QM/MM models are often used in connection with the molecular simulation techniques [19–23]. Monte Carlo or molecular dynamics (MD) simulations are employed to explore the configurational phase space of the molecular system under study. Then, QM/MM calculations of a molecular property in question are performed on a number of molecular solute–solvent configurations. The final liquid-phase result is obtained as a statistical average over the molecular configurations. Such integrated modelling scheme combining classical MD simulations and QM/MM methods has been succesfully used previously by us to address the tautomeric equilibrium of adenine through predictions of its tautomer-averaged ^{15}N NMR spectrum [11] and also to study other molecular systems with the inherent fast chemical exchange. For example, we have elucidated the molecular self-association of liquid acetic acid [24], rationalized the composition dependence of the ^{1}H NMR chemical shift of exchanging protons in the aqueous mixtures of choline lysinate ionic liquid [25], and studied ion paring effects in the dilute solutions of 1-butyl-3-methylimidazolium chloride ionic liquid [26].

The focus of the present contribution is on the tautomeric equilibrium of mycotoxin citrinin in the dichloromethane (DCM) solution. Citrinin is a secondary metabolite of some fungi of genera *Penicillium*, *Aspergillus* and *Monascus*, often found together with the nephrotoxic ochratoxin A. First identified in 1931 after it was extracted from *Penicillium citrinum* fungus [27], citrinin was found to possess antibacterial properties. However, citrinin's toxicity to mammalian cells was soon discovered [28], and enthusiasm for conducting further research of the properties of this compound has quickly diminished. The exact mechanism of citrinin's toxicity is still not clear, although the main pathway is considered to be related to the oxidative stress and the suppression of existing antioxidants in the cells, such as glutathione. Recently, the interest in citrinin as well as its metabolites has risen due to their potential anti-inflamatory, anticancer and neuroprotective properties [29–31]. In addition, it has become increasingly relevant to develop reliable means of

the detection of even miniscule amounts of citrinin in food products and living organisms [32, 33], so as to prevent food poisoning caused by citrinin found in stored grains [34], beans, fruits and fruit juice, other plant-based products, and spoiled dairy products [35].

Citrinin in the solid state as well as in an inert solution such as DCM exists as a mixture of two tautomers – *para*-quinone methide and *ortho*-quinone methide, see Fig. 1, referred to as, respectively, *p*-citrinin and *o*-citrinin in the following [36–38]. The tautomerization of citrinin in the solid state has been studied well, and the tautomeric equilibrium constant of around 0.5 has been established at room temperature by X-ray diffraction and ^{13}C NMR measurements, in favour of the *p*-citrinin form [37, 39, 40]. The tautomeric equilibrium in solution is less understood, partly because citrinin in certain solvents like methanol or water is unstable [37, 41]. In the dichloromethane solution, the ratio of *p*-citrinin and *o*-citrinin has been estimated to be around 4:3 at room temperature based on the measured temperature dependences of ^{13}C NMR spectra [37]. Surprisingly, the ^{17}O NMR spectrum of citrinin in dichloromethane showed virtually no temperature dependence, thus preventing a reliable derivation of the equilibrium populations of *p*- and *o*-citrinin tautomers in this case. We are here determined to predict the ^{17}O NMR spectra of tautomeric forms of citrinin in the dichloromethane solution by using the integrated computational scheme that combines classical MD simulations and the linear-response QM/MM approach for NMR isotropic shielding constants. In addition to *p*- and *o*-citrinin tautomers, we will also consider the endiol form of citrinin shown in Fig. 1(c), which was studied previously using computational methods [42]. The knowledge of the tautomeric equilibrium of citrinin in the solution is of importance for understanding the mechanism of its cytotoxicity and other biological or potential pharmacological functions [43].

2. Methods

2.1. Molecular dynamics simulations

MD simulations of two systems were conducted in this work – *p*- and *o*-citrinin in the dichloromethane solution at infinite dilution conditions. The liquid-phase geometries of *p*-citrinin, *o*-citrinin and dichloromethane molecules were derived by geometry optimization employing the B3LYP density functional [44], the aug-cc-pVTZ one-electron basis set [45] and the PCM model [13, 46] to account for solute–solvent interactions. Optimizations of the geometries were performed using the Gaussian16 program [47] along with tightened criteria for convergence as well as an ultrafine grid for 2-electron integrals. The structures of all the molecules were kept rigid in the MD simulations. Atomic point charges of *p*-citrinin, *o*-citrinin and DCM molecules were calculated using a CHELPG procedure [48] at the B3LYP/aug-cc-pVTZ level of theory, imposing constraints on the dipole moment and employing the PCM model to account for the dichloromethane environment for each molecule. Intermolecular van der Waals interactions were modelled by the 6-12-type Lennard-Jones potential. The Lennard-Jones parameters were selected from the OPLS force field for citrinin [49] and DCM [50] molecules, and Lorentz–Berthelot

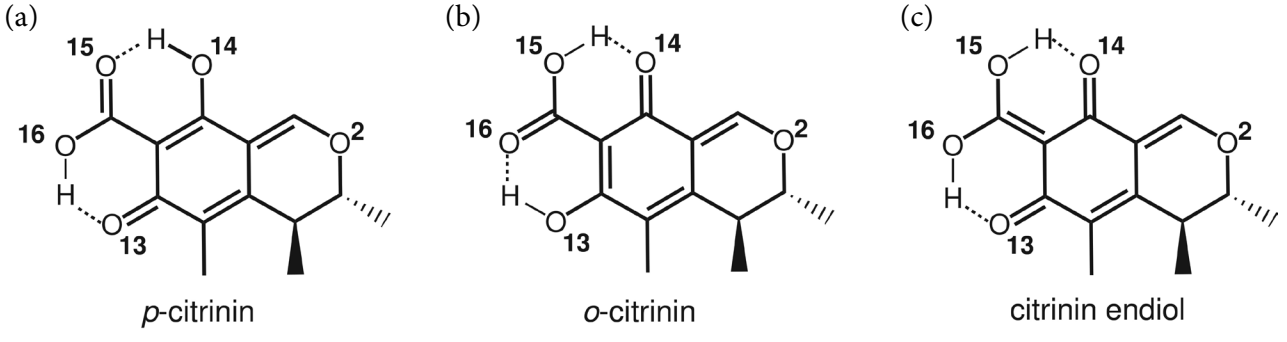

Fig. 1. The *para*-quinone methide (a), *ortho*-quinone methide (b) and endiol (c) tautomers of citrinin. Also included is atom labelling in citrinin following Ref. [37].

mixing rules were utilized. Molecular dynamics simulations were performed using the MolSim 3.3.0 program [51].

The systems simulated in this work consisted of a single *p*- or *o*-citrinin molecule and 500 DCM molecules. Periodic boundary conditions were used for simulations in the cubic box with cut-off distances for intermolecular Coulomb and van der Waals interactions set to half of the box side length. Newton's equations of motion were integrated using the velocity Verlet method [52] with an integration step of 1 fs. A Berendsen barostat and thermostat [53] were used to maintain a constant pressure of 1 atm and temperature of 298.15 K, respectively.

To achieve thermodynamic equilibrium conditions, the MD simulation of each system was first performed in the NPT ensemble for 300 ps, which was sufficient to achieve converged mass densities. The resulting cubic box side lengths were 38.04 and 38.32 Å for the DCM solution of *p*-citrinin and *o*-citrinin, respectively. The equilibration phase was continued in the NVT ensemble for another 500 ps, followed by 2 ns NVT production run. Molecular configurations were sampled every 10 ps, and the trajectory files therefore contained 200 snapshots for each system to be considered in the structural analysis. Reduced sets of 100 molecular configurations were used for subsequent QM/MM calculations of NMR isotropic shielding constants.

2.2. QM/MM calculations

To compute the ^{17}O NMR chemical shifts of citrinin, we relied on the polarizable linear-response QM/MM model based on the density functional theory [18, 21, 54] that is implemented in the electronic structure program Dalton2019 [55]. Gauge-origin including orbitals were used to assure origin-independent NMR shielding tensors. The quantum mechanical part (QM) of the system was described by the PBE0 exchange-correlation functional [56] along with the def2-TZVP basis set [57]. Two different molecular mechanics (MM) force fields (FF) were considered for the solvent molecules in the classical region. The non-polarizable FF for DCM molecules includes the same atomic point charges as used in the MD simulations (*vide supra*). The polarizable FF for DCM molecules includes atomic point charges as well as atomic isotropic dipole polarizabilities. The point charges were derived using the CHELPG procedure with the constraint on the dipole moment for the liquid-phase geometries of DCM but using in-vacuum electronic densities computed at the B3LYP/aug-cc-pVTZ level of theory. The isotropic dipole polarizabilities were calculated according to the LoProp method [58] using the B3LYP functional and the aug-cc-pVTZ basis set that was recontracted to be of atomic natural orbital type as required by the LoProp method.

For either system, four different series of QM/MM calculations were conducted. In the first series labelled Run1, the QM region included sole citrinin, while all solvent molecules were described by the nonpolarizable potential. In the series labelled Run2, the QM region was expanded by 5 solvent molecules selected in each configuration based on their proximity to the oxygen atoms in citrinin, i.e. one DCM molecule closest to each of the five oxygen atoms. In the series labelled Run3, the QM region was further expanded by now including 2 closest DCM molecules to each oxygen atom of citrinin, thus 10 in total. Finally in the series labelled Run4, the QM region of each configuration was exactly like in the series Run2, but classical solvent molecules were described by the polarizable potential instead. The solvent molecules to be included to the QM/MM calculation were selected by considering a spherical cut-off radius of 15 Å, centred at the centre of mass of citrinin. The final liquid-phase results for ^{17}O NMR isotropic shielding constants were determined as statistical averages over 100 molecular configurations, and the statistical errors were evaluated as standard deviations of the sample.

2.3. Constant of tautomeric equilibrium

To determine the tautomeric equilibrium between the tautomers of citrinin in the DCM solution, the constants of tautomeric equilibrium pK_T were calculated using the so-called thermodynamic cycle approach as described in previous works [59–61]. The Gibbs free energies in the gas phase and in the dichloromethane solution were calculated at 298 K for *p*-citrinin, *o*-citrinin and citrinin endiol using the M05-2X density functional [62] and cc-pVTZ basis set [45] together with the implicit

solvation model based on density (SMD) [63] to account for solvation. The Gaussian16 program was used for all calculations of free energies.

3. Results and discussion

3.1. Constant of tautomeric equilibrium

A straightforward way to quantify the tautomeric equilibrium in the solution using electronic structure methods is through the predictions of the Gibbs free energy change of the tautomerization reaction in the gas phase as well as solvation free energies of the two interconverting tautomers [59, 60]. These thermodynamic quantities are then combined to calculate the Gibbs free energy change of the tautomerization reaction in the liquid phase according to the thermodynamic cycle, and that allows calculating the logarithmic equilibrium constant of tautomeric conversion pK_T. However, in order to calculate pK_T with the accuracy of one log-unit, the free energy change of the tauromerization reaction should be calculated with an error of 1.37 kcal/mol at room temperature only. It is difficult to reach such precision for energies of isolated molecules, achievable only by correlated *ab initio* methods, let alone of those in the condensed phases. Therefore, the accuracy of the quantum chemical predictions for pK_T's of a few log-units is quite common [64].

The pK_T value of 0.12 for *o*-citrinin relative to *p*-citrinin in the DCM solution was reported based on experimental ^{13}C NMR measurements at room temperature [37], indicating that the two tautomers are nearly energetically equivalent, with a slight preference for *p*-citrinin. The corresponding value of pK_T computed in this work using the thermodynamic cycle approach is –0.04, thus predicting the populations of the *p*- and *o*-citrinin tautomers to be virtually equal in DCM, with a very small preference for the *o*-citrinin tautomer. Having in mind the typical uncertainty of 1–2 logarithmic units in the quantum chemical predictions of pK_T, the agreement between the theoretical and experimental values of pK_T achieved here is to be considered as remarkably good.

We have also attempted to predict the pK_T for the endiol tautomer of citrinin w.r.t. *p*-citrinin. The difference in the electronic energy of endiol citrinin relative to that of the most stable *p*-citrinin tautomer in the gas phase has been reported to be around 10.4 kJ/mol, calculated using the B3LYP functional and 6-311++G(2d,2p) basis set [42]. The corresponding value computed at the M05-2X/cc-pVTZ level in this work is 6.29 kJ/mol, leading to a similar conclusion that both *p*- and *o*-citrinin tautomers are considerably more stable than endiol in the gas phase. Furthermore, the endiol tautomeric form of citrinin was found to be unstable in the DCM solution modelled by SMD, evolving to either the *p*- or *o*-citrinin form during the geometry optimization. On this ground, the pK_T for the endiol tautomer could not be calculated, and the endiol tautomer has not been considered in the remainder of this work.

3.2. MD simulations

To inspect the structural distribution of the DCM solvent molecules around the citrinin solute, radial distribution functions (RDFs) between oxygen atoms in the tautomers of citrinin and hydrogen atoms in DCM molecules have been computed and depicted in Fig. 2. DCM is a solvent of medium polarity and it has poor capabilities for hydrogen bonding, and this is reflected in relatively unstructured shapes of the RDFs seen in Fig. 2. That is particularly evident in Fig. 2(a) showing no trace of any specific hydrogen bonding interaction between the ether oxygen atom O2 in *p*- or *o*-citrinin and DCM molecules. Due to the tautomeric shift, the O13/O15 and O14/O16 switch their character between the carbonyl- and hydroxyl-type in *p*-citrinin and *o*-citrinin. As seen in Fig. 2(b–e), the distribution of DCM molecules in the first coordination shell of carbonyl oxygen atoms in *p*- or *o*-citrinin has the most pronounced character, possibly forming a weak hydrogen bonding in these cases. The distribution of solvent molecules around hydroxyl oxygen atoms of citrinin is rather similar to that seen around the ether oxygen atom O2, and resembles the unstructured distribution typical for inert solvents.

3.3. QM/MM calculations

The ^{17}O NMR isotropic magnetic shielding constants of *p*-citrinin and *o*-citrinin computed using the QM/MM approaches are collected in Table 1.

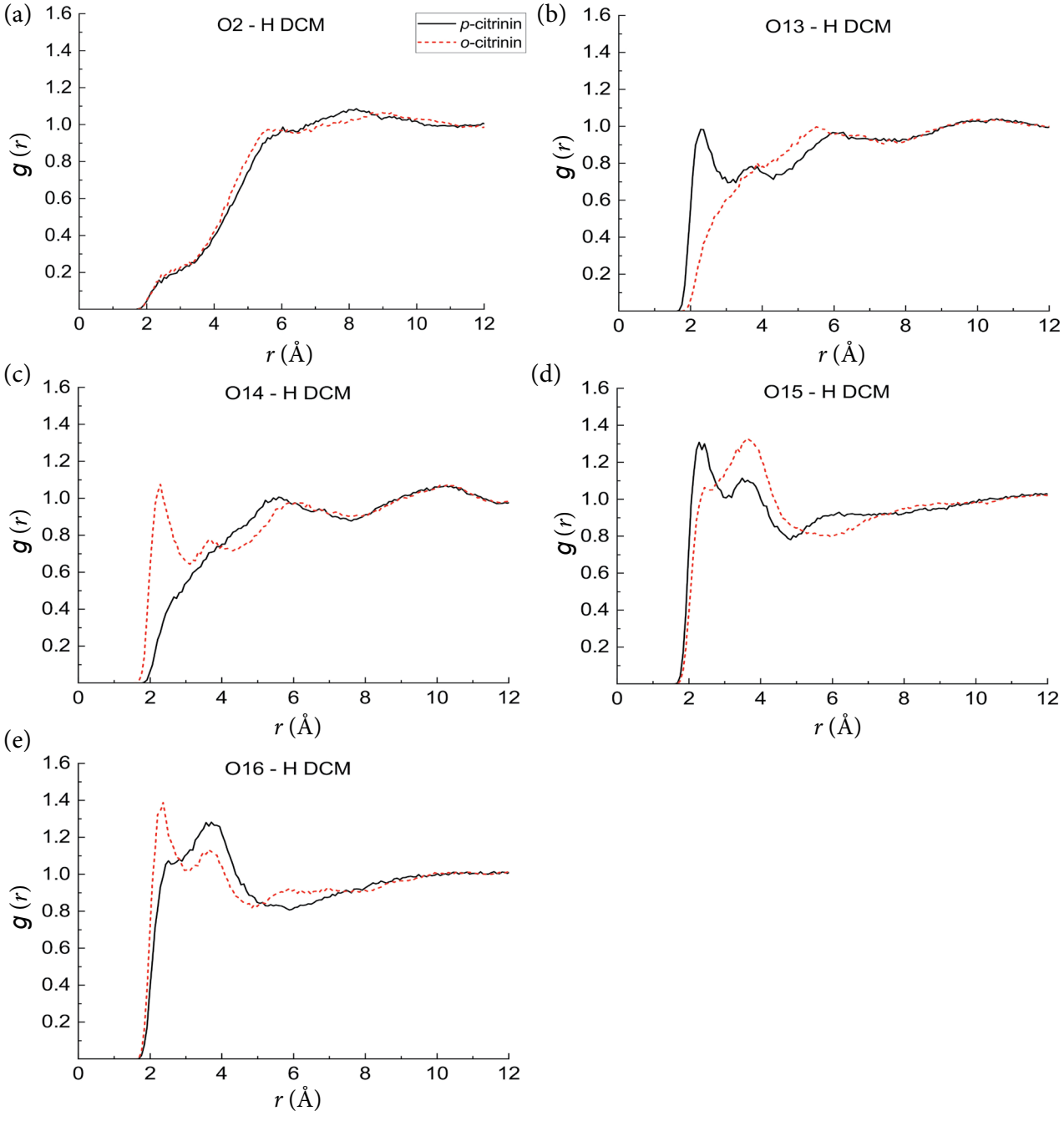

Fig. 2. Radial distribution functions between oxygen atoms of *p*-citrinin and *o*-citrinin and hydrogen atoms of dichloromethane. Refer to Fig. 1 for atom labelling.

In addition, we have calculated the ^{17}O NMR shieldings of the two tautomers of citrinin using their condensed-phase geometries but neglecting their interactions with the solvent molecules altogether. Thus, the obtained results are included in Table 1 under the label 'in vacuum' in the 2nd column, and they will serve as a reference to quantitatively assess the direct solvent effect on the magnetic shielding constants of citrinin in the solution. As seen in Table 1, the direct solvent effect on the ^{17}O NMR shieldings of citrinin is qualitatively different for specific types of an oxygen atom. For the ether oxygen atom, the shielding is seen to decrease by around 12–14 ppm due to the direct effect of the solvent modelled as point charges, while the shielding constants of carbonyl oxygen atoms have increased by around 20–30 ppm in this case. The shielding constant of hydroxyl oxygen atom has been comparatively little affected by the direct solvent effect, leading to an increase of the value by around 1–8 ppm.

Table 1. The QM/MM results for the ^{17}O NMR isotropic shielding constants σ of the oxygen atoms of *p*-citrinin and *o*-citrinin tautomers given in units of ppm as averages over 100 molecular configurations. For each entry of σ, the standard deviation of the sample (SD) has been provided. Refer to the main text for the description of different series of QM/MM calculations performed in this work. Refer to Fig. 1 for atom labelling.

Tautomer	Series	O2		O13		O14		O15		O16	
		σ	SD	σ	SD	σ	SD	σ	SD	σ	SD
p-citrinin	in vacuum	134.35	–	–105.54	–	172.66	–	–25.69	–	101.03	–
	Run1	120.23	0.51	–73.22	1.19	173.26	0.48	–6.35	0.75	108.59	0.42
	Run2	117.99	0.53	–72.94	1.23	169.78	0.52	–9.83	0.71	104.51	0.41
	Run3	117.32	0.52	–73.96	1.25	167.95	0.55	–11.52	0.76	102.50	0.44
	Run4	119.30	0.48	–75.19	1.12	169.65	0.50	–11.21	0.66	104.06	0.39
o-citrinin	in vacuum	134.15	–	137.05	–	–32.59	–	101.65	–	–21.63	–
	Run1	121.98	0.53	140.24	0.53	–7.28	1.06	109.53	0.44	–2.24	0.65
	Run2	119.47	0.58	136.89	0.63	–8.67	1.08	105.47	0.45	–5.73	0.66
	Run3	118.78	0.60	135.09	0.66	–9.50	1.07	103.45	0.49	–7.77	0.67
	Run4	120.44	0.54	136.59	0.59	–10.38	1.00	104.86	0.42	–7.04	0.61

The extension of the QM region to include some solvent molecules around the solute offers an improved description of electrostatic and polarization intermolecular interactions, and, in addition, introduces non-classical effects such as Pauli repulsion and dispersion. The comparison of the results between the QM/MM series Run1 and Run2 in Table 1 reveals that the inclusion of five DCM solvent molecules to the QM region of the model leads to a small decrease by up to around 4 ppm of all shielding constants of oxygen atoms in *p*- or *o*-citrinin. Furthermore, the computational results of series Run2 can be considered to be the fairly converged w.r.t. number of quantum-mechanically described solvent molecules, as further expansion of the QM region by including 10 DCM molecules leads to further reduction of the shielding constants by no more than around 2 ppm. Finally, we have also used the polarizable potential for classical DCM molecules by also retaining 5 closest DCM molecules to the five oxygen atom sites in citrinin, thus introducing the full nonlinear many-body description of solute–solvent polarization. The comparison of the results of QM/MM series Run2 and Run4 shows that direct polarization interactions lead to a small reduction of shieldings of carbonyl oxygen atoms and a small increase of those for ether oxygen atoms, while the shielding constants of hydroxyl oxygens remain barely affected.

The computational results for the ^{17}O NMR chemical shifts of citrinin are based on the shielding constants of QM/MM series Run4, our best estimate obtained using the most elaborate model. In Fig. 3, we show our computational results of the relative ^{17}O NMR spectra of *p*- or *o*-citrinin tautomers in the DCM solution. The computed spectra of either *p*-citrinin or *o*-citrinin not at all resemble the shape of the measured relative ^{17}O NMR spectrum of citrinin in DCM [37] shown in Fig. 4(a), signifying that tautomerism is indeed in action and cannot be ignored. The qualitative shape of the ^{17}O NMR

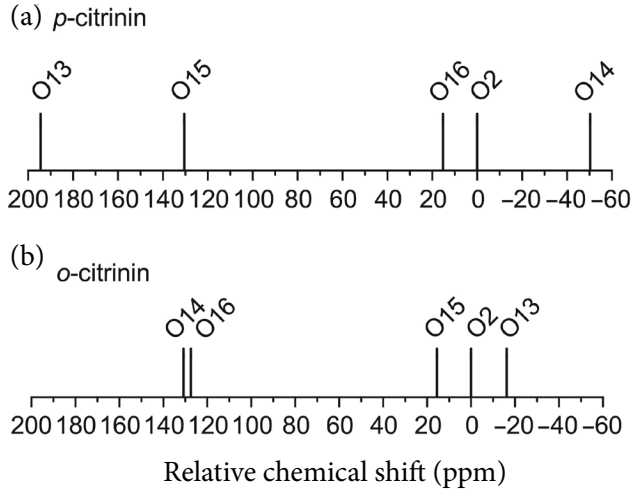

Fig. 3. QM/MM-based relative ^{17}O NMR spectra of *p*-citrinin (a) and *o*-citrinin (b) in the dichloromethane solution. The NMR shielding constant of the O2 atom has been chosen as an internal reference. Refer to Fig. 1 for atom labelling.

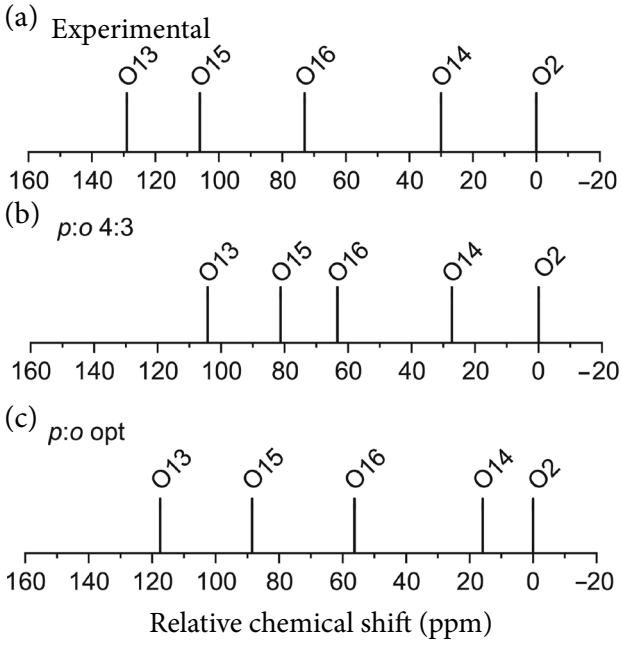

Fig. 4. (a) Experimental relative ^{17}O NMR spectrum of citrinin in the dichloromethane solution, constructed using data in Ref. [37]. (b) QM/MM-based tautomer-averaged relative ^{17}O NMR spectrum of citrinin in dichloromethane, constructed using the experimentally determined equilibrium ratio of *p*-citrinin and *o*-citrinin tautomers of 4-to-3. (c) QM/MM-based tautomer-averaged relative ^{17}O NMR spectrum of citrinin in dichloromethane, constructed using the optimized ratio of *p*-citrinin and *o*-citrinin tautomers of around 7-to-4. The NMR shielding constant of the O2 atom has been chosen as an internal reference in all cases.

spectrum of citrinin in the DCM solution is recovered by using tautomer-averaged shielding constants according to Eq. (1) and the experimentally determined tautomeric equilibrium constant of *p*- and *o*-citrinin of 0.75 [37], see Fig. 4(b). As seen in Fig. 4(c), he quantitative agreement between computational and experimental spectra has been further improved by optimizing the equilibrium ratio of the two tautomers in the solution via the minimization of the score function

$$F = \Sigma(\delta^{obs} - \delta^{comp})^2. \quad (2)$$

In this equation, δ^{obs} and δ^{comp} are, respectively, the experimentally observed and computed relative ^{17}O NMR chemical shifts of citrinin in the DCM solution, and the summation runs over all 5 oxygen sites in citrinin. The optimization procedure leads to the tautomeric ratio of 7:4 for *p*-citrinin and *o*-citrinin tautomers in the DCM solution. Our computational estimate of the equilibrium constant of *p*- and *o*-citrinin in the DCM solution of 0.57 agrees with the experimentally measured value of 0.75 extremely well. It is noteworthy that the relative positioning of the NMR signals of oxygen atoms O13 to O16 has been recovered by our computations very accurately even in quantitative terms as compared to experimental data, compare Figs. 4(a) and (c). Only the separation between the chemical shifts of ether oxygen atom O2 and that of O14 has been clearly underestimated. A likely cause of this discrepancy could potentially be attributed to the inaccuracies in the force field used to describe this particular oxygen atom type in the MD simulations [65].

4. Summary

The tautomeric equilibrium of citrinin in dichloromethane was studied in this work using the classical molecular dynamics simulations and combined linear-response QM/MM calculations of the ^{17}O NMR shielding constants. The MD simulations have shown that solvent distribution around the *para*-quinone methide and *ortho*-quinone methide tautomers of citrinin is rather uniform, as is typical for inert solvents without hydrogen bonding capabilities, and even the solvent structuring around the electronegative oxygen atoms of citrinin is barely pronounced. The QM/MM calculations have shown that a significant amount of the direct solvent effect on the NMR isotropic shielding constants of oxygen in citrinin is due to the electrostatic solute–solvent interactions, although non-classical effects and direct many-body polarization interactions should be accounted for as well. The optimization of the tautomeric ratio between *p*- and *o*-citrinin tautomers was carried out aiming to obtain the best quantitative agreement between the experimental and QM/MM-based relative ^{17}O NMR spectra of citrinin in the DCM solution. The computed tautomeric ratio of 7:4 for *p*-citrinin and *o*-citrinin tautomers agrees with the corresponding experimental ratio of 4:3 very well, signifying the near-thermodynamic equivalence of the *p*-citrinin and *o*-citrinin tautomers in the DCM solution, with a very slight preference for the *p*-citrinin tautomeric form. The thermodynamic cycle-based quantum

chemical calculation of the tautomeric equilibrium constant of citrinin in DCM leads to the virtually identical conclusion, although the quantitative result of the equilibrium constant should be regarded as less reliable than that based on computated NMR spectroscopic data. Our attempt to include the endiol tautomer of citrinin showed that this tautomer is not stable in the solution modelled by the dielectric continuum approach. Therefore, endiol tautomer is not expected to be formed in the dichloromethane solution of citrinin and thus does not contribute to the observed NMR spectra.

Acknowledgements

K.A. is indebted to Professor Vytautas Balevičius for introducing him to the field of computational molecular spectroscopy and for many years of fruitful scientific collaboration. Computations were performed on the resources provided by the High Performance Computing Center 'HPC Saulėtekis' at Vilnius University, Lithuania. This work has received support from the Research Council of Lithuania, Grant No. S-MIP-22-74. Authors thank COST Action No. CA21101.

References

[1] A. Lesage, Recent advances in solid-state NMR spectroscopy of spin $I = 1/2$ nuclei, Phys. Chem. Chem. Phys. **11**, 6876 (2009).

[2] O. Pecher, J. Carretero-Gonzalez, K.J. Griffith, and C.P. Grey, Materials' methods: NMR in battery research, Chem. Mater. **29**, 213 (2016).

[3] B. Reif, S.E. Ashbrook, L. Emsley, and M. Hong, Solid-state NMR spectroscopy, Nat. Rev. Methods Primers **1**, 1 (2021).

[4] S. Ahlawat, K.R. Mote, N. Lakomek, and V. Agarwal, Solid-state NMR: methods for biological solids, Chem. Rev. **122**, 9643 (2022).

[5] M. Renault, A. Cukkemane, and M. Baldus, Solid-state NMR spectroscopy on complex biomolecules, Angew. Chem., Int. Ed. **49**, 8346 (2010).

[6] J. Keeler. *Understanding NMR Spectroscopy*, 2nd ed. (Wiley, Chichester, 2010).

[7] R.M. Claramunt, C. López, M.D. Santa María, D. Sanz, and J. Elguero, The use of NMR spectroscopy to study tautomerism, Prog. Nucl. Magn. Reson. Spectrosc. **49**, 169 (2006).

[8] G. Gocheva, N. Petkov, A. Garcia Luri, S. Iliev, N. Ivanova, J. Petrova, Y. Mitrev, G. Madjarova, and A. Ivanova, Tautomerism in folic acid: Combined molecular modelling and NMR study, J. Mol. Liq. **292**, 111392 (2019).

[9] K. Bártová, I. Císařová, A. Lyčka, and M. Dračínský, Tautomerism of azo dyes in the solid state studied by ^{15}N, ^{14}N, ^{13}and ^{1}H NMR spectroscopy, X-ray diffraction and quantum-chemical calculations, Dye. Pigment. **178**, 108342 (2020).

[10] A.C.F. de Albuquerque, G.S. Corrêa, G.T. Albuquerque, F.L.P. Costa, L.T. Costa, M.R. Lage, J.W. de M. Carneiro, and F.M. dos S. Junior, Theoretical study of keto-enol tautomerism in 7-*epi*-clusianone by quantum chemical calculations of NMR chemical shifts, J. Mol. Model. **28**, 239 (2022).

[11] K. Aidas, K.V. Mikkelsen, and J. Kongsted, On the existence of the H3 tautomer of adenine in aqueous solution. Rationalizations based on hybrid quantum mechanics/molecular mechanics predictions, Phys. Chem. Chem. Phys. **12**, 761 (2010).

[12] J. Tomasi and M. Persico, Molecular interactions in solution: An overview of methods based on continuous distributions of the solvent, Chem. Rev. **94**, 2027 (1994).

[13] J. Tomasi, B. Mennucci, and R. Cammi, Quantum mechanical continuum solvation models, Chem. Rev. **105**, 2999 (2005).

[14] A. Klamt and G. Schüürmann, COSMO: A new approach to dielectric screening in solvents with explicit expressions for the screening energy and its gradient, J. Chem. Soc. Perkin Trans. **2**, 799 (1993).

[15] K. Kitaura and K. Morokuma, A new energy decomposition scheme for molecular interactions within the Hartree-Fock approximation, Int. J. Quantum Chem. **10**, 325 (1976).

[16] A. Warshel and M. Levitt, Theoretical studies of enzymic reactions: Dielectric, electrostatic and steric stabilization of the carbonium ion in the reaction of lysozyme, J. Mol. Biol. **103**, 227 (1976).

[17] J. Kongsted, A. Osted, K.V. Mikkelsen, and O. Christiansen, The QM/MM approach for wavefunctions, energies and response functions within self-consistent field and coupled cluster theories, Mol. Phys. **100**, 1813 (2002).

[18] J.M. Olsen, K. Aidas, and J. Kongsted, Excited states in solution through polarizable embedding, J. Chem. Theory Comput. **6**, 3721 (2010).

[19] H.C. Georg, K. Coutinho, and S. Canuto, Converged electronic polarization of acetone in liquid water and the role in the n–π^* transition, Chem. Phys. Lett. **429**, 119 (2006).

[20] N. Arul Murugan, J. Kongsted, Z. Rinkevicius, and H. Ågren, Breakdown of the first hyperpolarizability/bond-length alternation parameter relationship, Proc. Natl. Acad. Sci. USA. **107**, 16453 (2010).

[21] C.B. Nielsen, O. Christiansen, K.V. Mikkelsen, and J. Kongsted, Density functional self-consistent quantum mechanics/molecular mechanics theory for linear and nonlinear molecular properties: Applications to solvated water and formaldehyde, J. Chem. Phys. **126**, 154112 (2007).

[22] T. Schwabe, J.M. Haugaard Olsen, K. Sneskov, J. Kongsted, and O. Christiansen, Solvation effects on electronic transitions: Exploring the performance of advanced solvent potentials in polarizable embedding calculations, J. Chem. Theory Comput. **7**, 2209 (2011).

[23] K. Aidas, A. Møgelhøj, H. Kjær, C.B. Nielsen, K.V. Mikkelsen, K. Ruud, O. Christiansen, and J. Kongsted, Solvent effects on NMR isotropic shielding constants. A comparison between explicit polarizable discrete and continuum approaches, J. Phys. Chem. A. **111**, 4199 (2007).

[24] D. Lengvinaitė, K. Aidas, and L. Kimtys, Molecular aggregation in liquid acetic acid: insight from molecular dynamics/quantum mechanics modelling of structural and NMR properties, Phys. Chem. Chem. Phys. **21**, 14811 (2019).

[25] E. Sipavičius, L. Mikalauskas, V. Klimavicius, and K. Aidas, Intermolecular organization in aqueous mixtures of choline lysinate studied via NMR and molecular dynamics/quantum mechanics, Phys. Chem. Chem. Phys. **27**, 14790 (2025).

[26] D. Lengvinaitė, V. Klimavičius, V. Balevicius, and K. Aidas, Computational NMR study of ion pairing of 1-decyl-3-methylimidazolium chloride in molecular solvents, J. Phys. Chem. B **124**, 10776 (2020).

[27] J.W.G. de Oliveira Filho, M.T. Islam, E.S. Ali, S.J. Uddin, J.V. de Oliveira Santos, M.V. Oliveira Barros de Alencar, A.L. Gomes Júnior, M.F. Correia Jardim Paz, M.d.R.M. de Brito, J.M. de Castro e Sousa, et al., A comprehensive review on biological properties of citrinin, Food Chem. Toxicol. **110**, 130 (2017).

[28] A.M. Ambrose, Some toxicological and pharmacological properties of citrinin, J. Pharmacol. Exp. Ther. **88**, 173 (1946).

[29] C.H. Chang, F.Y. Yu, L.T. Wang, Y.S. Lin, and B.H. Liu, Activation of ERK and JNK signaling pathways by mycotoxin citrinin in human cells, Toxicol. Appl. Pharmacol. **237**, 281 (2009).

[30] Y. Nakajima, H. Iguchi, S. Kamisuki, F. Sugawara, T. Furuichi, and Y. Shinoda, Low doses of the mycotoxin citrinin protect cortical neurons against glutamate-induced excitotoxicity, J. Toxicol. Sci. **41**, 311 (2016).

[31] A.-A.P. de Menezes, R.P.S. Aguiar, J.O. Santos, C. Sarkar, M.T. Islam, A.L. Braga, M.M. Hasan, F.C.C. da Silva, J. Sharifi-Rad, A. Dey, D. Calina, A.A.C. Melo-Cavalcante, and J.M.C. Sousa, Citrinin as a potential anti-cancer therapy: A comprehensive review, Chem. Biol. Interact. **381**, 110561 (2023).

[32] N. Atar, M.L. Yola, and T. Eren, Sensitive determination of citrinin based on molecular imprinted electrochemical sensor, Appl. Surf. Sci. **362**, 315 (2016).

[33] G.H. Degen, N. Ali, and U. Gundert-Remy, Preliminary data on citrinin kinetics in humans and their use to estimate citrinin exposure based on biomarkers, Toxicol. Lett. **282**, 43 (2018).

[34] D. Abramson, R. Hulasare, R.K. York, N.D.G. White, and D.S. Jayas, Mycotoxins, ergosterol, and odor volatiles in durum wheat during granary storage at 16% and 20% moisture content, J. Stored Prod. Res. **41**, 67 (2005).

[35] EFSA Panel on Contaminants in the Food Chain (CONTAM), Scientific opinion on the risks for

public and animal health related to the presence of citrinin in food and feed, EFSA J. **10**, 2605 (2012).

[36] U. Sankawa, Y. Ebizuka, H. Noguchi, Y. Isikawa, S. Kitaghawa, Y. Yamamoto, T. Kobayashi, Y. Iitak, and H. Seto, Biosynthesis of citrinin in *aspergillus terreus*: Incorporation studies with [2-^{13}C, 2-$^{2}H_3$], [1-^{13}C, $^{18}O_2$] and [1-^{13}C, ^{17}O]-acetate, Tetrahedron **39**, 3583 (1983).

[37] R. Poupko, Z. Luz, and R. Destro, Carbon-13 NMR of citrinin in the solid state and in solutions, J. Phys. Chem. A **101**, 5097 (1997).

[38] M.H. Lauer, M.H. Gehlen, K. de Jesus, and R.G.S. Berlinck, Fluorescence spectroscopy and confocal microscopy of the mycotoxin citrinin in condensed phase and hydrogel films, J. Fluoresc. **24**, 745 (2014).

[39] R. Destro and R.E. Marsh, Temperature dependence of tautomeric equilibria in the solid state: The case of citrinin, J. Am. Chem. Soc. **106**, 7269 (1984).

[40] R. Destro, Proton transfer in the solid state: Therymodynamic parameters from an X-ray study in the temperature range 20–293 K, Chem. Phys. Lett. **181**, 232 (1991).

[41] J. Barber, J.L. Cornford, T.D. Howard, and D. Sharples, The structure of citrinin *in vivo*, J. Chem. Soc. Perkin Trans. **00**, 2743 (1987).

[42] M. Appell, D. Moravec, and W.B. Bosma, Quantum chemical study of the structure and properties of citrinin, Mol. Simulat. **38**, 284 (2012).

[43] P.V. Bharatam, O.R. Valanju, A.A. Wani, and D.K. Dhaked, Importance of tautomerism in drugs, Drug Discov. Today **28**, 103494 (2023).

[44] A.D. Becke, Density-functional thermochemistry. III. The role of exact exchange, J. Chem. Phys. **98**, 5648 (1993).

[45] R.A. Kendall, T.H. Dunning, and R.J. Harrison, Electron affinities of the first-row atoms revisited. Systematic basis sets and wave functions, J. Chem. Phys. **96**, 6796 (1992).

[46] V. Barone, M. Cossi, and J. Tomasi, Geometry optimization of molecular structures in solution by the polarizable continuum model, J. Comput. Chem. **19**, 404 (1998).

[47] M.J. Frisch, G.W. Trucks, H.B. Schlegel, G.E. Scuseria, M.A. Robb, J.R. Cheeseman, G. Scalmani, V. Barone, G.A. Petersson, H. Nakatsuji, et al., *Gaussian 16, Revision c.01* (Gaussian Inc., Wallingford, CT, 2026).

[48] C.M. Breneman and K.B. Wiberg, Determining atom-centered monopoles from molecular electrostatic potentials. The need for high sampling density in formamide conformational analysis, J. Comp. Chem. **11**, 361 (1990).

[49] W.L. Jorgensen, D.S. Maxwell, and J. Tirado-Rives, Determining atom-centered monopoles from molecular electrostatic potentials. The need for high sampling density in formamide conformational analysis, J. Am. Chem. Soc. **118**, 11225 (1996).

[50] D. Lim, W.L. Jorgensen, D.A. Hrovat, and W.T. Borden, Solvent effects on the ring opening of cyclopropanones to oxyallyls: A combined ab initio and Monte Carlo study, J. Am. Chem. Soc. **116**, 3494 (1994).

[51] J. Reščič and P. Linse, MOLSIM: A modular molecular simulation software, J. Comp. Chem. **36**, 1259 (2015).

[52] L. Verlet, Computer 'experiments' on classical fluids. I. Thermodynamical properties of Lennard-Jones molecules, Phys. Rev. **159**, 98 (1967).

[53] H.J.C. Berendsen, J.P.M. Postma, W.F. van Gunsteren, A. DiNola, and J.R. Haak, Molecular dynamics with coupling to an external bath, J. Chem. Phys. **81**, 3684 (1984).

[54] J. Kongsted, C.B. Nielsen, K.V. Mikkelsen, O. Christiansen, and K. Ruud, Nuclear magnetic shielding constants of liquid water: Insights from hybrid quantum mechanics/molecular mechanics models, J. Chem. Phys. **126**, 034510 (2007).

[55] K. Aidas, C. Angeli, K.L. Bak, V. Bakken, R. Bast, L. Boman, O. Christiansen, R. Cimiraglia, S. Coriani, P. Dahle, et al., The Dalton quantum chemistry program system, WIREs Comput. Mol. Sci. **4**, 269 (2014).

[56] C. Adamo and V. Barone, Toward reliable density functional methods without adjustable parameters: The PBE0 model, J. Chem. Phys. **110**, 6158 (1999).

[57] F. Weigend and R. Ahlrichs, Balanced basis sets of split valence, triple zeta valence and quadruple zeta valence quality for H to Rn: Design and assessment of accuracy, Phys. Chem. Chem. Phys. **7**, 3297 (2005).

[58] L. Gagliardi, R. Lindh, and G. Karlström, Local properties of quantum chemical systems: The LoProp approach, J. Chem. Phys. **121**, 4494 (2004).

[59] A. Cedillo, S. Kvedaravičiūtė, and K. Aidas, Prediction of the tautomer stability and acidity of phenacylpyridines in aqueous solution, Theor. Chem. Acc. **139**, 52 (2020).

[60] Y.C. Martin, Let's not forget tautomers, J. Comput. Aided Mol. Des. **23**, 693 (2009).

[61] Ž. Murnikova, V. Klimavicius, F. Mocci, A. Laaksonen, and K. Aidas, On the mechanism behind the enhanced solubility of glibenclamide in aqueous ionic liquid solution, J. Mol. Liq. **422**, 127153 (2025).

[62] Y. Zhao, N.E. Schultz, and D.G. Truhlar, Density functional for spectroscopy: No long-range self-interaction error, good performance for Rydberg and charge-transfer states, and better performance on average than B3LYP for ground states, J. Chem. Theory Comput. **2**, 364(2006).

[63] A.V. Marenich, C.J. Cramer, and D.G. Truhlar, Universal solvation model based on solute electron density and on a continuum model of the solvent defined by the bulk dielectric constant and atomic surface tensions, J. Phys. Chem. B **113**, 6378 (2009).

[64] R.F. Ribeiro, A.V. Marenich, C.J. Cramer, and D.G. Truhlar, Prediction of SAMPL2 aqueous solvation free energies and tautomeric ratios using the SM8, SM8AD, and SMD solvation models, J. Comput. Aided Mol. Des. **24**, 317 (2010).

[65] J.J. Eriksen, J.M.H. Olsen, K. Aidas, H. Ågren, K.V. Mikkelsen, and J. Kongsted, Computational protocols for prediction of solute NMR relative chemical shifts. A case study of L-tryptophan in aqueous solution, J. Comp. Chem. **32**, 2853 (2011).

MIKOTOKSINO CITRININO TAUTOMERINĖ PUSIAUSVYRA DICHLORMETANO TIRPALE: ^{17}O BMR SPEKTRŲ MODELIAVIMAS MOLEKULINĖS DINAMIKOS SIMULIACIJOMIS IR KVANTINĖS MECHANIKOS METODAIS

Ž. Murnikova, K. Aidas

Vilniaus universiteto Fizikos fakulteto Cheminės fizikos institutas, Vilnius, Lietuva

Santrauka

Modeliuota mikotoksino citrinino tautomerinė pusiausvyra dichlormetano tirpale naudojant klasikines molekulių dinamikos (MD) simuliacijas bei ^{17}O branduolių magnetinio rezonanso (BMR) ekranavimo konstantų skaičiavimus. MD simuliacijos atskleidė, kad dichlormetano tirpiklio molekulių pasiskirstymas aplink *para*- ar *orto*-chinono metido citrinino tautomerus yra mažai struktūrizuotas, ko ir galima tikėtis atsižvelgiant į tai, kad dichlormetanas yra vidutinio poliškumo, vandenilinių ryšių suformuoti negalintis tirpiklis. Naudojant jungtinius kvantinės mechanikos ir molekulinės mechanikos metodus buvo apskaičiuotos *p*- ir *o*-citrinino tautomerų ^{17}O BMR ekranavimo konstantos dichlormetano tirpale. Remiantis šių skaičiavimų rezultatais, buvo sumodeliuotas suvidurkintas citrinino ^{17}O BMR spektras, kuris su eksperimentiniu spektru sutapo geriausiai tada, kai pusiausvirasis *p*- ir *o*-citrinino tautomerų santykis buvo lygus 7:4. Šis apskaičiuotas santykis labai gerai sutapo su nustatytu eksperimentiškai, lygiu 4:3. Tai rodo, kad abu citrinino tautomerai yra praktiškai energetiškai lygiaverčiai dichlormetano tirpale, pusiausvyrai mažumėlę pasislinkus į *para*-chinono metido tautomero pusę. Darbe taip pat buvo bandoma įvertinti endiolio tautomero įtaką citrinino ^{17}O BMR spektrui. Vis dėlto šis tautomeras nėra stabilus dichlormetano tirpiklyje, kai modeliuojama dielektrinio kontinuumo metodu. Tikėtina, kad citrinino endiolio tautomeras dichlormetano tirpale nesiformuoja ir neturi įtakos jo BMR spektrams.